Heliyon 6 (2020) e03482

Contents lists available at ScienceDirect

Heliyon

journal homepage: www.cell.com/heliyon

Research article

Non periodic oscillations, bistability, coexistence of chaos and hyperchaos in the simplest resistorless Op-Amp based Colpitts oscillator

R. Zebaze Nanfa'a [a,b], R. Tchitnga [a,b,c,*], P.H. Louodop Fotso [a,b,d], R. Kengne [a,b], F.C. Talla [a,b,e], B. Nana [b,e], F.B. Pelap [f]

[a] Unité de Recherche de Matière Condensée d'Electronique et de Traitement du Signal (URMACETS), Department of Physics, Faculty of Science, University of Dschang, P.O. Box 67 Dschang, Cameroon
[b] Research Group on Experimental and Applied Physics for Sustainable Development, Department of Physics, Faculty of Science, University of Dschang, P.O.Box 412 Dschang, Cameroon
[c] Institute of Surface Chemistry and Catalysis, University of Ulm, Albert-Einstein-Allee 47, 89081, Ulm, Germany
[d] São Paulo State University (UNESP), Instituto de Física Teórica, Rua Dr. Bento Teobaldo Ferraz 271, Bloco II, Barra Funda, 01140-070, São Paulo, Brazil
[e] Department of Physics, University of Bamenda, Bamenda, P.O.Box 39 Bamenda, Cameroon
[f] Laboratoire de Mécanique et de Modélisation des Systèmes, L2MS, Department of Physics, Faculty of Science, University of Dschang, P.O.Box 67, Dschang, Cameroon

ARTICLE INFO

Keywords:
Electrical engineering
Nonlinear physics
Operational amplifier
High frequency
Parasitic capacitances
Hyperchaos
Bistability

ABSTRACT

In the framework of a project on simple circuits with unexpected high degrees of freedom, we report an autonomous microwave oscillator made of a CLC linear resonator of Colpitts type and a single general purpose operational amplifier (Op-Amp). The resonator is in a parallel coupling with the Op-Amp to build the necessary feedback loop of the oscillator. Unlike the general topology of Op-Amp-based oscillators found in the literature including almost always the presence of a negative resistance to justify the nonlinear oscillatory behavior of such circuits, our zero resistor circuit exhibits chaotic and hyperchaotic signals in GHz frequency domain, as well as many other features of complex dynamic systems, including bistability. This simplest form of Colpitts oscillator is adequate to be used as didactic model for the study of complex systems at undergraduate level. Analog and experimental results are proposed.

1. Introduction

The search for secure communication using chaos has led to the development of hyperchaotic systems, which have revealed to be more complex, with higher degree of freedom, than their chaotic counterparts. The increasing number of works on encryption using hyperchaotic signals reinforces their importance [1, 2, 3, 4].

Experimental hyperchaotic circuits in the literature result either from modified chaotic circuits consisting in the extension of the number of energy tanks to more than three for autonomous ones [5, 6, 7], coupling of at least two chaotic circuits for synchronization purpose or coupling in networks [8, 9, 10, 11], driving 3D systems to higher complexity [12, 13] or even analog development from mathematic equations of hyperchaotic systems [14].

In each of these cases, it appears that simple stand-alone hyperchaotic circuits with very reduced number of components are very few [15]. The same as it has been established since the renowned Chua's circuit [16] that autonomous chaotic circuits without time delay cannot exist unless they carry at least three energy tanks, it is not expected that autonomous hyperchaotic circuits carrying less than four of such components exist.

In the frame work of the present paper, we aim at showing that as a real physically two-component circuit made of a field effect transistor and a tapped coil has led to chaos [17], it is also possible, under particular attention, to find coexistence of chaos and hyperchaos in a real physically four-component autonomous circuit which on one hand can be used as simple didactic model [18, 19, 20]. At the same time, on the other hand, it fits into engineering systems with applications based on chaos and hyperchaos, and can therefore be used in secure communication [1, 2, 11, 21, 22], in pseudo and true random bit generation [23, 24], for the study of complex bifurcations [25, 26], as well as for the simulation of collective motion of huge group of individuals such as flock of birds [27], just to name some.

* Corresponding author.
E-mail address: robert.tchitnga@eaphysud.org (R. Tchitnga).

https://doi.org/10.1016/j.heliyon.2020.e03482
Received 5 May 2019; Received in revised form 23 December 2019; Accepted 20 February 2020
2405-8440/© 2020 Published by Elsevier Ltd. This is an open access article under the CC BY-NC-ND license (http://creativecommons.org/licenses/by-nc-nd/4.0/).

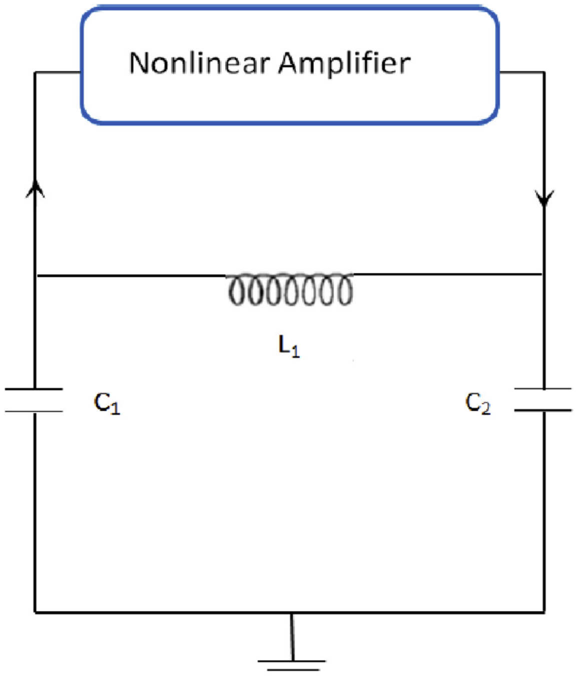

Figure 1. General structure of the Colpitts oscillator.

In a recent article entitled "*A simple RLCC-Diode-OpAmp chaotic oscillator*" [28], the authors proposed an autonomous Op-Amp-based circuit in which they inserted a floating diode in parallel to the existing linear and nonlinear blocks, in order to generate chaotic behavior. They justified the presence of the diode by asserting that it was to avoid the use of an additional Op-Amp with high gain or a current source. A deep observation shows that this oscillator is of Colpitts type because of the presence of a CLC linear resonator in the circuit.

In the same journal three years prior to the above mentioned reference however, Sprott already proposed a standard for the publication of new chaotic systems [29]. This includes that they should fulfill at least one of the three following criteria:

(i) The system should credibly model some important unsolved problem in nature and shed insight on that problem;
(ii) The system should exhibit some behavior previously unobserved;
(iii) The system should be simpler than all other known examples exhibiting the observed behavior.

In view of the conditions set by Sprott, it seemed necessary to review the circuit of Ref. [18] by removing all redundant components and find out which particular complex dynamics it can still exhibit in its most reduced form. The Colpitts form should therefore be preserved and considered as candidate circuit to make sure that the modification will not alter the basic structure of the reviewed circuit.

The Colpitts oscillator is an old electronic circuit dating from 1915-1918 [30] and having the particularity of being made of a CLC resonator in which one electrode of each capacitor is put at the mass while the remaining electrodes are connected to each end of the same coil (Figure 1). Its structure is well known and studied [31]. Although the Colpitts circuit is already a century old oscillator, it is still very actual [32]. In recent years, there have been numerous works on Colpitts circuits some of which very cumbersome because of the number of peripheral components that must constitute the nonlinear amplifier responsible for the birth of oscillations [33, 34, 35, 36]. Many operational amplifier-based Colpitts oscillators use a built-in negative resistor to inject the non-linear signal responsible for generating oscillations in the feedback loop [31, 37]. Although the use of negative resistance generally leads to impressive results [38, 39], we would challenge to use only the CLC resonator and one Op-Amp to produce an autonomous Colpitts like chaotic and hyperchaotic oscillator, which is one of the aims of this paper.

The next aim of our paper is to study other advantageous dynamics this simplest Op-Amp based autonomous circuit can have compared to the cumbersome ones. The key question remains here whether it is necessary to insert other nonlinear or active components in the circuit just in order to induce chaos as done by Ref [28], when one of the component, say the Op-Amp, is already an active and at the same times a nonlinear element. Further aim of the study of this simple circuit is to reveal that, when the processed signals are of high frequencies and strongly nonlinear, a general purpose Op-Amp with voltage feedback (VFA) can adopt a behavior which is reserved to Op-Amps with current feedback (CFA). To the best of our knowledge, this has not been shown before.

As modern electronics tends to reduce the number of lab modules [40] and the power consummation [41], is it possible to find a high frequency Colpitts oscillator with the nonlinear amplifier devoid of any other passive components than those forming the resonator? If yes, this can be a very simplified didactical model of nonlinear circuit, fulfilling therefore the third condition set by Sprott [29].

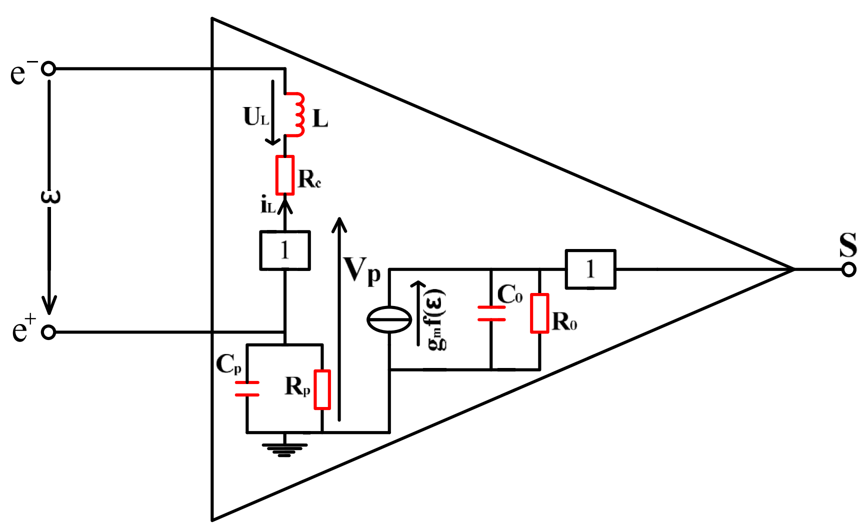

Figure 2. Novel equivalent circuit of a general purpose Op-Amp. Operating at high frequency [42].

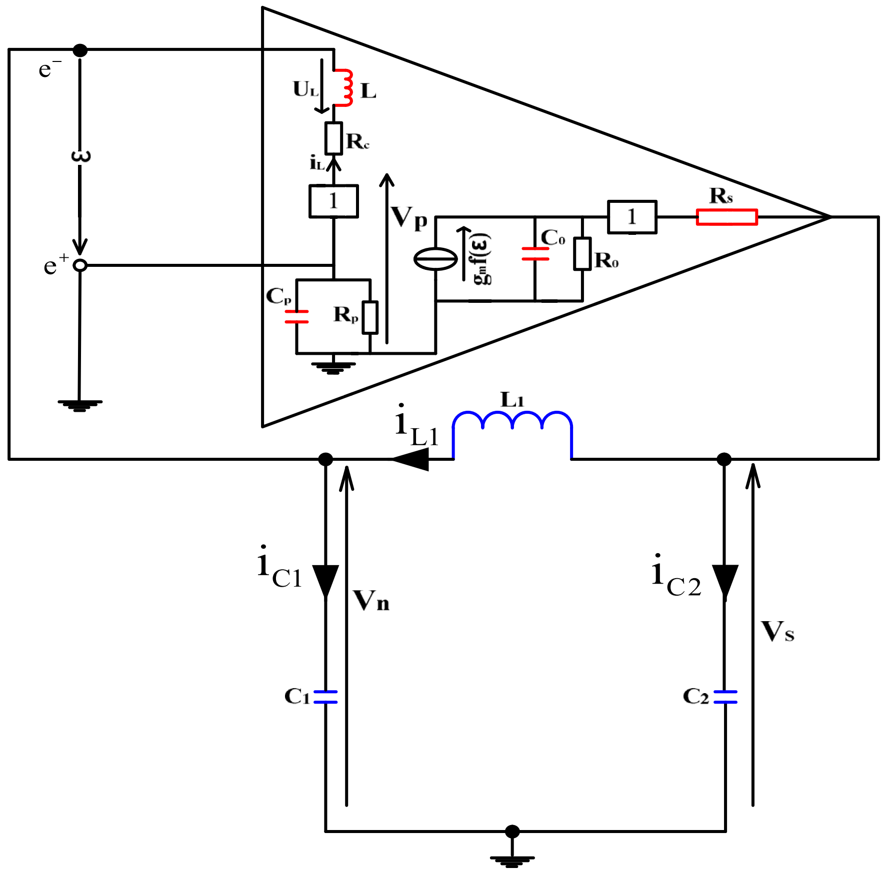

Figure 3. Overall equivalent circuit of the resistorless oscillator operating at high frequency using a light extended version of the Op-Amp model in Ref. [42].

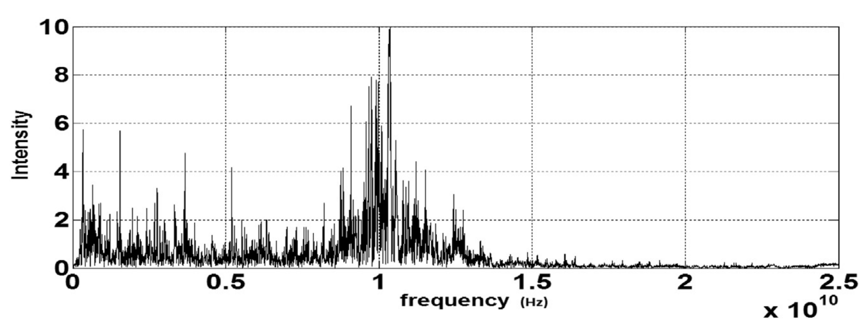

Figure 4. Frequency spectrum of the resistorless Op-Amp-based oscillator obtained from numerical simulations under MatLab for 10,000 samples with a normalized sampling frequency of $f_s = 2 \times 10^7$ Hz and the parameter $\eta = 77.50$.

Taking into account the fact that CLC tanks generally lead to high frequency oscillations in circuits, we considered the nonlinear amplifier of Figure 1 to be made solely of a single general purpose Op-Amp. We use the novel high frequency model (Figure 2) recently proposed by some of us [42] to design and study the resulting resistorless four-component circuit (Figure 1) with equivalent circuit given in Figure 3. While it has already been shown that autonomous resistorless transistor based-circuits can deliver chaotic signals [17], to the best of our knowledge, no autonomous zero resistor chaotic circuit in the category of general purpose Op-Amp-based oscillators has been reported so far. One of such circuit, but with rather a minimal number of resistors is the experimental circuit by Yim et ***al.*** with only one effective resistance [43]. It is also a four-element circuit, but exhibiting simply a chaotic signal.

It is worth remaindering that electronic components generally behave differently in different frequency domains [44, 45]. It has been proven that at high frequency, operational amplifiers develop parasitic virtual components which, in some cases have to be compensated by adding real components in the overall circuit to avoid alteration of the expected signals [46]. This leads us to wonder whether it could be possible to study the structure of a Colpitts oscillator using only a general purpose operational amplifier as a nonlinear amplifier and taking into account the high frequency structure of this later, then exploiting the related properties and behaviors.

In Ref. [42], the authors highlighted unsuspected chaotic oscillations in the Op-Amp relaxation oscillator with help of the circuit model in Figure 2. The results obtained are quite relevant. Figure 3 using that same model represents the high frequency simplest Op-Amp-based Colpitts oscillator. A light modification of the first version of high frequency Op-Amp by Tchitnga et ***al.*** [42] through the presence of a new element, the passive internal resistor $0.0\Omega \leq R_S \leq 100\Omega$, is justified by the fact that a reactive component is directly connected to the output of the operational amplifier [46].

After developing the mathematical model of the new oscillator and determine the oscillation conditions, we will study the dynamics of the

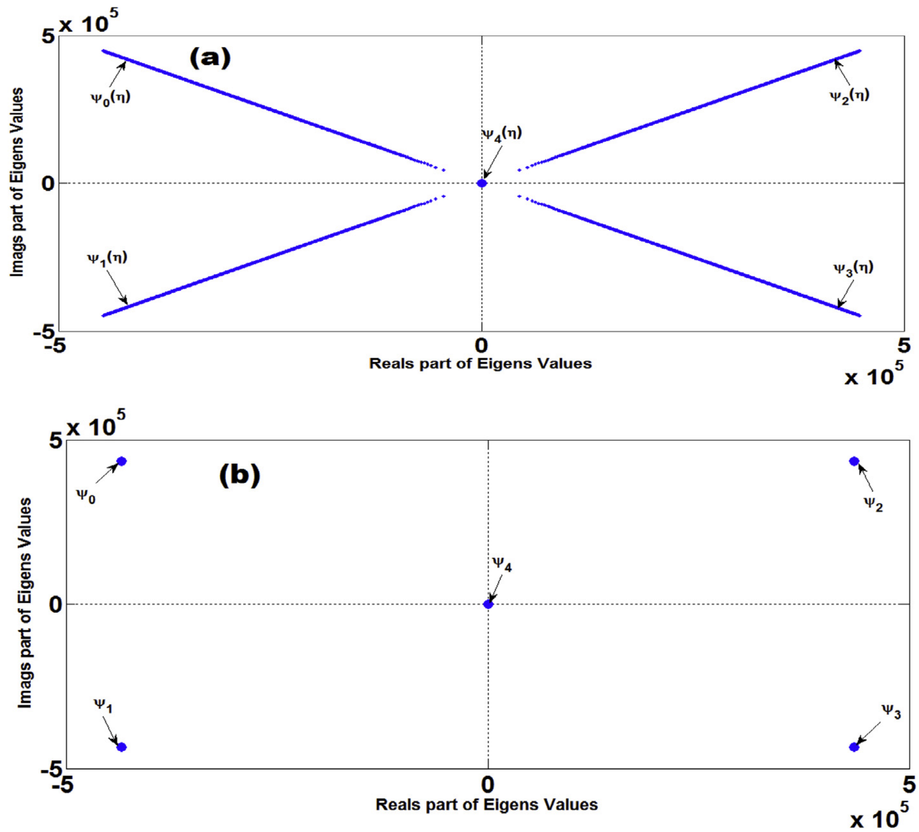

Figure 5. Set of eigenvalues related to the characteristic polynomial $G(\psi)$ (a) for the control parameter varying in the range $30 \leq \eta \leq 100$ and (b) for the fixed value of the control parameter $\eta = 84.06$.

circuit to understand its various unsuspected complex behavior including hyperchaos and bistability. The third part of the paper will consist of the presentation of the numerical (MatLab) and analogs (PSpice) results as well as lab experimental ones. The concluding part of the paper opens a gate to outcomes inviting to revisit the modeling of some high-frequency Op-Amp-based circuits that have never been deeply explored, but can still hide subtle uncovered dynamics.

2. High frequency structure of the resistorless Op-Amp-based oscillator

2.1. Mathematical model and frequency spectrum

First suppose the circuit of Figure 1 oscillates at high frequency. Then, the novel high frequency model of Op-Amp by Tchitnga et *al*. [42] can be used to describe the equivalent circuit in Figure 3. The Kirchoff's laws applied to that circuit will lead to the following states equations:

$$\begin{cases} C_0\dfrac{dV_0}{dt} = g_m f(\varepsilon) - \dfrac{V_0}{R_0} \\ C_2\dfrac{dV_s}{dt} = \dfrac{V_0 - V_s}{R_s} - i_{L_1} \\ C_1\dfrac{dV_n}{dt} = i_{L_1} - i_L \\ L\dfrac{di_L}{dt} = V_n - R_C i_L \\ L_1\dfrac{di_{L_1}}{dt} = V_s - V_n \end{cases} \tag{1}$$

Here, L and C_0 are the parasitic inductance and capacitance of the Op-Amp when the circuit oscillate at high frequency. g_m is its trans-conductance. For a detailed description of the model, the reader should refer to Ref. [42]. The non-linearity of the operational amplifier is defined by [47] as

$$f(\varepsilon) = V_s(\varepsilon) = V_{Sat}\tanh\left(\frac{a_0\varepsilon}{V_{Sat}}\right) \tag{2}$$

V_{sat} is the maximum voltage at the output of the Op-Amp when it is biased with $\pm V_{cc}$; a_0 is its open-loop gain, meanwhile its trans-conductance is given by Eq. (3).

$$g_m = \sqrt{\frac{1}{R_0^2} + (C_0\omega_0)^2} \tag{3}$$

The state variables of the oscillator and time can be respectively normalized by the reference voltage V_{sat}, $\frac{V_{sat}}{R_i}$ $(i = 1, 2)$ and $\tau = f_r \times t$, with $f_r = 7.81 \times 10^2 \times f_z$. The term f_z given by Eq. (4) is the natural frequency of the Colpitts oscillator [48] and more generally of CLC circuit types:

$$f_z = \frac{1}{2\pi\sqrt{\frac{(C_1 \times C_2)}{(C_1 + C_2)}L_1}} \tag{4}$$

Introducing the dimensionless variables.

x_1 to x_5 as $x_1 = \frac{V_0}{V_{Sat}}K_1$, $x_2 = \frac{V_s}{V_{Sat}}K_2$, $x_3 = \frac{V_n}{V_{Sat}}K_3$, $x_4 = \frac{R_1 i_L}{V_{Sat}}K_4$, $x_5 = \frac{R_2 i_{L_1}}{V_{Sat}}K_5$ and $\frac{t}{\tau} = \frac{1}{f_r}$ into Eq. (1), the dimensionless mathematical model of our oscillator at high frequency becomes the asymmetric system below:

$$\begin{cases} \dot{x}_1(\tau) = \alpha\tanh(-a_0 x_3) - \beta x_1 \\ \dot{x}_2(\tau) = \gamma(x_1 - x_2) - \theta x_5 \\ \dot{x}_3(\tau) = \eta(x_5 - x_4) \\ \dot{x}_4(\tau) = \xi x_3 - \overline{\eta} x_4 \\ \dot{x}_5(\tau) = \overline{\xi}(x_2 - x_3) \end{cases} \tag{5}$$

The parameters in Eq. (5) are defined as:

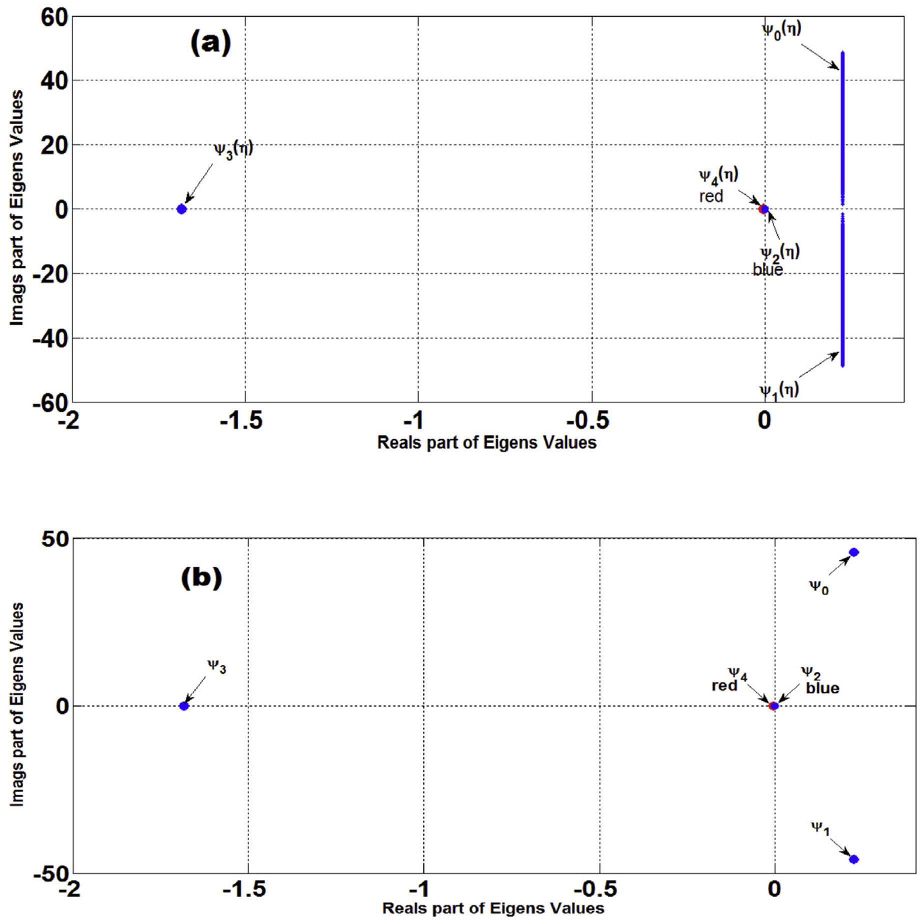

Figure 6. Set of eigenvalues related to the characteristic polynomial $H(\psi)$ (a) for the control parameter in the range $30 \leq \eta \leq 100$ and (b) for the fixed value of the control parameter $\eta = 84.06$.

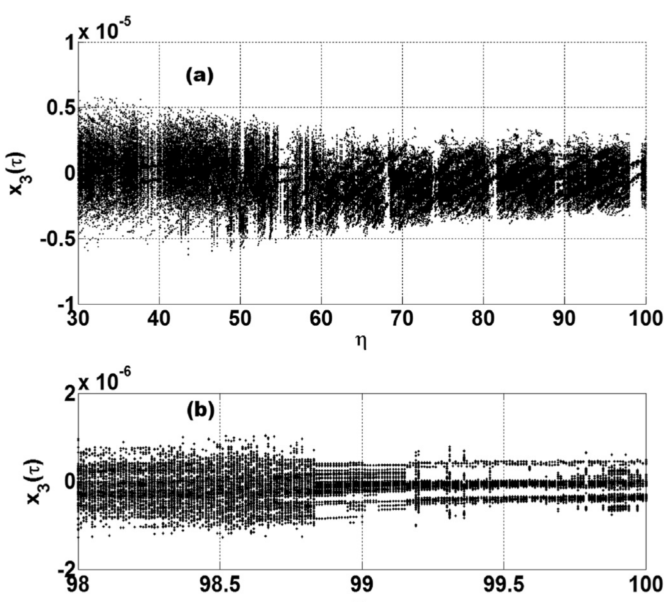

Figure 7. Bifurcation diagrams of the high frequency resistorless Op-Amp based oscillator obtained by plotting the maximal local of x_3 for the initial conditions $x_0 = (0.65, 0.75, 0.65, 0.08, 0.08)$. For (a), the control parameter is taken in the range $30 \leq \eta \leq 100$, while (b) depicts the zoom of a tiny region of the previous picture for $(98 \leq \eta \leq 100)$.

$\alpha = \frac{g_m}{C_0 f_r}$, $\beta = \frac{1}{C_0 R_0 f_r}$, $\gamma = \frac{R_2}{R_S}\theta$, $\theta = \frac{1}{C_2 R_2 f_r}$, $\eta = \frac{1}{C_1 R_1 f_r}$, $\xi = \frac{R_1}{L f_r} K_4$, $\overline{\eta} = \frac{R_C}{L f_r}$, and $\overline{\xi} = \frac{R_2}{L_1 f_r}$; with $K_1 = K_2 = K_3 = K_5 = 1$ and $K_4 = 3 \times 10^4$. The dimensionless constants $K_i (i = 1, 2, 3, 4, 5)$ are used to harmonize numeric values (MatLab) and analog investigations (P-Spice). Inductances being extreme sensitive elements to current variations, we will use parameters related to capacitors to control the system. From the two external capacitors in the circuit (Figure 3) we choose C_1 for reasons of simplicity because it is related to a single parameter η, while C_2 depends on both γ and θ.

To validate the model, we adopt following internal components values for the Op-Amp as proposed by Ref. [46, 49]: $L = 1\mu H$; $a_0 = 10^{20}$; $g_m = 0.1\Omega^{-1}$; $R_0 = 10^9\Omega$; $C_0 = 1pF$; $r = 4.5\Omega$; $R_S = 0.144\Omega$. If we vary the control parameter η in the interval $30 \leq \eta \leq 100$, while keeping the external components at $L_1 = 1mH$; $C_2 = 340nF$; $R_1 = 0.09R_S$; $R_2 = 0.23R_S$ and $fr = 1 \times 10^7$, a MatLab simulation delivers the Fast Fourier Transform (FFT) for 10,000 samples, with a sampling frequency of $f_s = 2 \times 10^7$ Hz (Figure 4). This representation shows that the normalized fundamental frequency is located at $f_0 = 10.3$ GHz. It can safely be confirmed that our oscillator oscillates in high frequency regime.

2.2. Equilibrium points and stability analysis

Setting the velocity of the system's state variables to zero leads to finding its equilibrium points, if they do exist [50]. In the present case, it means finding the solutions of system (6):

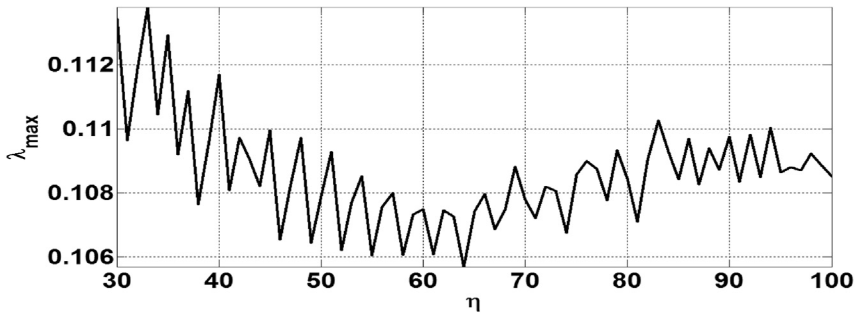

Figure 8. Maximum Lyapunov exponent for the high frequency oscillator corresponding to the bifurcation diagram in Figure 7 for the same variations of the control parameter and initial conditions.

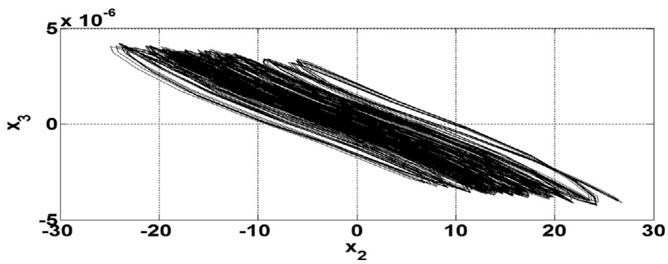

Figure 9. Phase diagram of the oscillator obtained for $\eta = 77.50$ corresponding to$C_1 = 99.25\text{nF}$ and initial conditions $x_0 = (0.65, 0.75, 0.65, 0.08, 0.08)$.

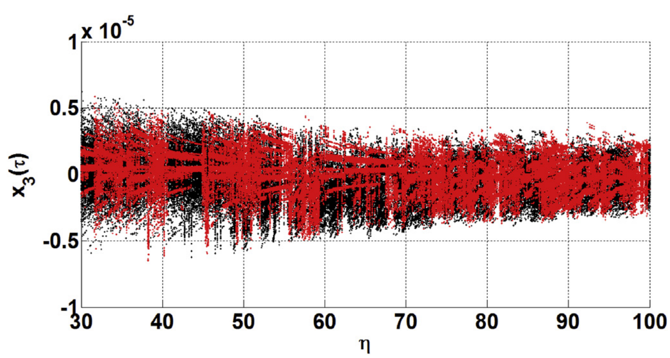

Figure 10. Bifurcation diagrams of the high frequency resistorless Op-Amp-based oscillator obtained by plotting the maximal local of x_3 with initial conditions $x_{01} = (0.65, 0.75, 0.65, 0.08, 0.08)$ for the black color and $x_{02} = (0.065, 0.075, 0.065, 0.008, 0.008)$ for the red color. The control parameter is taken in the range $30 \le \eta \le 100$.

$$\begin{cases} \alpha\tanh(-a_0x_3) - \beta x_1 = 0 \\ \gamma(x_1 - x_2) - \theta x_5 = 0 \\ \eta(x_5 - x_4) = 0 \\ \xi x_3 - \overline{\eta} x_4 = 0 \\ \overline{\xi}(x_2 - x_3) = 0 \end{cases} \tag{6}$$

The numerical resolution of this equation reveals two equilibrium points which are: the trivial equilibrium point

$$P_0(0, 0, 0, 0, 0) \tag{7}$$

and the non-trivial one,

$$P\left(\frac{\alpha}{\beta}, \frac{\overline{\eta}\gamma}{\theta\xi + \overline{\eta}\gamma}\frac{\alpha}{\beta}, \frac{\overline{\eta}\gamma}{\theta\xi + \overline{\eta}\gamma}\frac{\alpha}{\beta}, \frac{\xi\gamma}{\theta\xi + \overline{\eta}\gamma}\frac{\alpha}{\beta}, \frac{\xi\gamma}{\theta\xi + \overline{\eta}\gamma}\frac{\alpha}{\beta}\right) \tag{8}$$

One of the methods for analyzing equilibrium points is the perturbation of the Jacobian matrix associated with the system under study [51]. The Jacobian matrix *Mj* of our system is given by Eq. (9):

$$Mj = \begin{pmatrix} -\beta & 0 & -\dfrac{ao \times \alpha}{\cosh^2(-ao \times x_3)} & 0 & 0 \\ \gamma & -\gamma & 0 & 0 & -\theta \\ 0 & 0 & 0 & -\eta & \eta \\ 0 & 0 & \xi & \overline{\eta} & 0 \\ 0 & \overline{\xi} & -\overline{\xi} & 0 & 0 \end{pmatrix} \tag{9}$$

2.2.1. Stability analysis around the equilibrium point P_0

If we perform this perturbation around equilibrium points P_0 in Eq. (7), we obtain the new Jacobian matrix Mj_0 for which the stability can be analyzed:

$$Mj_0 = \begin{pmatrix} -\beta & 0 & -a_0\alpha & 0 & 0 \\ \gamma & -\gamma & 0 & 0 & -\theta \\ 0 & 0 & 0 & -\eta & \eta \\ 0 & 0 & \xi & \overline{\eta} & 0 \\ 0 & \overline{\xi} & -\overline{\xi} & 0 & 0 \end{pmatrix} \tag{10}$$

Its eigenvalues are solutions of the five order nonlinear algebraic Eq. (12), obtained by solving Eq. (11):

$$\det(Mj_0 - \psi I_d) = 0 \tag{11}$$

here ψ is the eigenvalue associated with this polynomial and I_d is the 5×5 identity matrix. Thus,

$$G(\psi) = G_5\psi^5 + G_4\psi^4 + G_3\psi^3 + G_2\psi^2 + G_1\psi + G_0 \tag{12}$$

Its parameters are defined by Eqs. (13), (14), (15), (16), (17), and (18):

$$G_5 = 1 \tag{13}$$

$$G_4 = \beta + \gamma - \overline{\eta} \tag{14}$$

$$G_3 = \beta\gamma - \beta\overline{\eta} - \gamma\overline{\eta} + \eta\xi + \eta\overline{\xi} + \theta\overline{\xi} \tag{15}$$

$$G_2 = -\beta\gamma\overline{\eta} + \beta\eta\xi + \beta\eta\overline{\xi} + \gamma\eta\xi + \gamma\eta\overline{\xi} + \beta\theta\overline{\xi} - \eta\overline{\eta}\overline{\xi} - \overline{\eta}\theta\overline{\xi} \tag{16}$$

$$G_1 = a_0\alpha\gamma\eta\overline{\xi} + \beta\gamma\eta\xi + \beta\gamma\eta\overline{\xi} - \beta\eta\overline{\eta}\overline{\xi} - \gamma\eta\overline{\eta}\overline{\xi} - \beta\overline{\eta}\theta\overline{\xi} + \eta\theta\xi\overline{\xi} \tag{17}$$

$$G_0 = -a_0\alpha\gamma\eta\overline{\eta}\overline{\xi} - \beta\gamma\eta\overline{\eta}\overline{\xi} + \beta\eta\theta\xi\overline{\xi} \tag{18}$$

Considering the internal and external elements' and parameters' values indicated in subsection 2.2, and varying the control parameter η in the interval $30 \le \eta \le 100$, we obtain Figure 5(a) which represents the set of eigenvalues resulting from the characteristic polynomial. It is worth noticing that, each single value of the control parameter yields just five

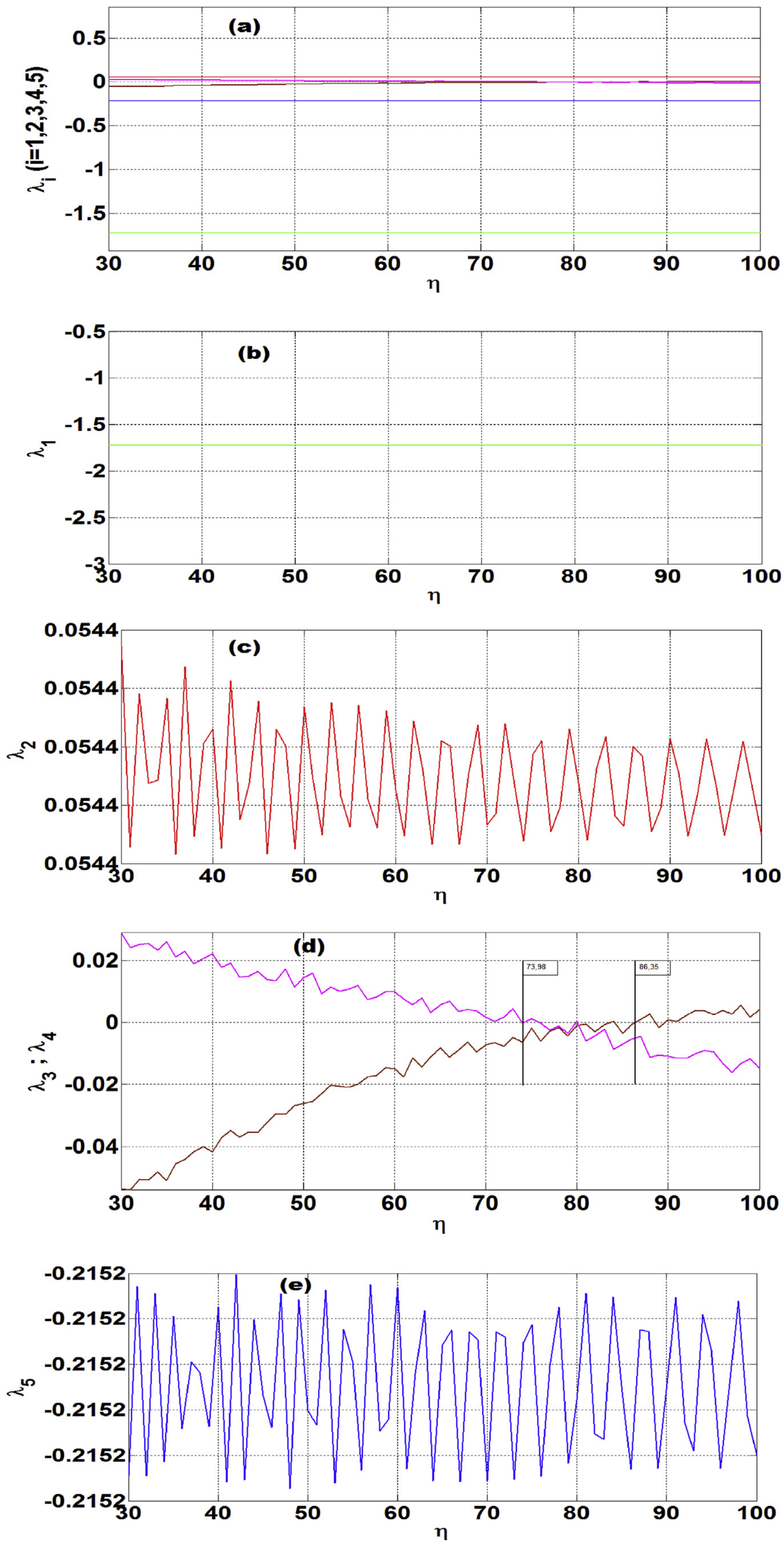

Figure 11. (a) Lyapunov exponents spectrum for the same variations of the control parameter $30 \leq \eta \leq 100$ with initial conditions $x_0 = (0.65, 0.75, 0.65, 0.08, 0.08)$; (b) First unidirectional Lyapunov exponent $\lambda_1 < 0$; (c) Second unidirectional Lyapunov exponent $\lambda_2 > 0$ means that the system is never periodic; (d) Third and fourth unidirectional Lyapunov exponents changing from positive to negative, defining hyperchaotic zones of type 1 and 2, and a window of chaotic oscillations; (e) Fifth unidirectional Lyapunov exponent.$\lambda_5 < 0$.

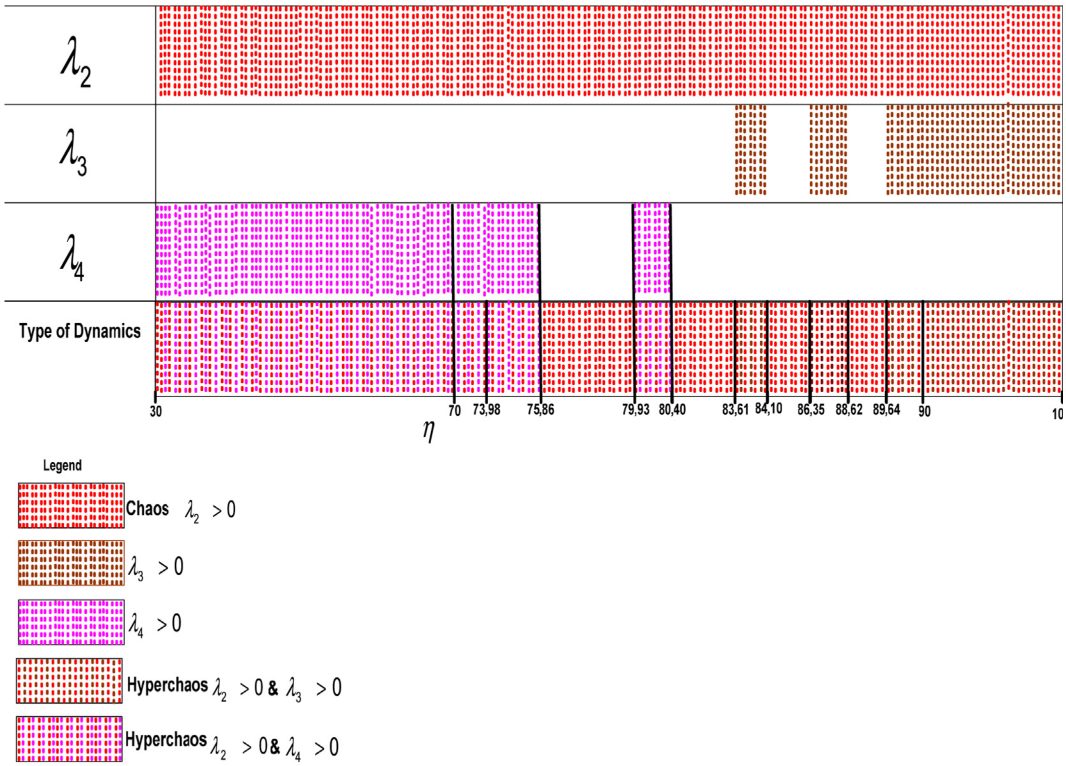

Figure 12. Chaotic ($\lambda_2 > 0$, red color) and hyperchaotic type 1 ($\lambda_2 > 0$ and $\lambda_3 > 0$, red + brown color) and type 2 ($\lambda_2 > 0$ and $\lambda_4 > 0$, red + purple color) regions according to the values taken by η.

points as the eigenvalues solution of the characteristic polynomial results from a 5 × 5 Matrix. Figure 5(b) depicts an example of visual solution for $\eta = 84.06$. The corresponding eigenvalues for that parameter value are: $\psi_0 = (-4.431 + 4.431i) \times 10^5$, $\psi_1 = (-4.431 - 4.431i) \times 10^5$, $\psi_2 = (4.431 + 4.431i) \times 10^5$, $\psi_3 = (4.431 - 4.431i) \times 10^5$, $\psi_4 = 45 \times 10^{-2}$.

It can be noted that some of the eigenvalues related to this characteristic polynomial are all complex numbers on one hand with positive real parts, while some others are complex conjugates with negative real parts. Therefore, according to the Routh-Hurwitz criterion P_0 is an unstable equilibrium point.

2.2.2. Stability analysis around the equilibrium point P_1

Proceeding as above for the perturbation of the second equilibrium point P_1 in Eq. (8) we obtain the Jacobian matrix Mj_1 for which the stability can also be analyzed:

$$Mj_1 = \begin{pmatrix} -\beta & 0 & -\dfrac{ao \times \alpha}{\cosh^2\left(-ao \times \dfrac{\overline{\eta}\gamma}{\theta\xi + \overline{\eta}\gamma}\dfrac{\alpha}{\beta}\right)} & 0 & 0 \\ \gamma & -\gamma & 0 & 0 & -\theta \\ 0 & 0 & 0 & -\eta & \eta \\ 0 & 0 & \xi & \overline{\eta} & 0 \\ 0 & \overline{\xi} & -\overline{\xi} & 0 & 0 \end{pmatrix} \tag{19}$$

Developing Eq. (20) which is

$$\det(Mj_1 - \psi I_d) = 0 \tag{20}$$

generates the characteristic polynomial of Mj_1 in the form of Eq. (21). ψ is the eigenvalue associated with this polynomial and I_d is the 5× 5 identity matrix:

$$H(\psi) = H_5\psi^5 + H_4\psi^4 + H_3\psi^3 + H_2\psi^2 + H_1\psi + H_0 \tag{21}$$

The parameters $H_i (i = 0, 1, 2, 3, 4, 5)$ are defined by Eqs. (22), (23), (24), (25), (26), and (27).

$$H_5 = 1 \tag{22}$$

$$H_4 = \beta + \gamma - \overline{\eta} \tag{23}$$

$$H_3 = \beta\gamma - \beta\overline{\eta} - \gamma\overline{\eta} + \eta\xi + \eta\overline{\xi} + \theta\overline{\xi} \tag{24}$$

$$H_2 = -\beta\gamma\overline{\eta} + \beta\eta\xi + \beta\eta\overline{\xi} + \gamma\eta\xi + \gamma\eta\overline{\xi} + \beta\theta\overline{\xi} - \eta\overline{\eta}\overline{\xi} - \overline{\eta}\theta\overline{\xi} \tag{25}$$

$$H_1 = \frac{ao \times \alpha}{\cosh^2\left(-ao \times \frac{\overline{\eta}\gamma}{\theta\xi + \overline{\eta}\gamma}\frac{\alpha}{\beta}\right)}\gamma\eta\overline{\xi} + \beta\gamma\eta\xi + \beta\gamma\eta\overline{\xi} - \beta\eta\overline{\eta}\overline{\xi} - \gamma\eta\overline{\eta}\overline{\xi} - \beta\overline{\eta}\theta\overline{\xi} + \eta\theta\xi\overline{\xi} \tag{26}$$

$$H_0 = -\frac{ao \times \alpha}{\cosh^2\left(-ao \times \frac{\overline{\eta}\gamma}{\theta\xi + \overline{\eta}\gamma}\frac{\alpha}{\beta}\right)}\gamma\eta\overline{\eta}\overline{\xi} - \beta\gamma\eta\overline{\eta}\overline{\xi} + \beta\eta\theta\xi\overline{\xi} \tag{27}$$

If we vary the parameter $30 \leq \eta \leq 100$ and consider all other parameters values as in the previous case, we obtain Figure 6(a) which represents the set of eigenvalues resulting from the characteristic polynomial around the fixed point P_1. On this graph, two real solutions are much closed to each other as it can better be revealed, if we plot the solution for a single value of the control parameter $\eta = 84.06$ (Figure 6(b)). Among the five points solution ψ_2(blue) and ψ_4(red) are almost superposed. For that fixed value of the parameter, the eigenvalues solutions are: $\psi_0 = 0.225 + 45.842i$, $\psi_1 = 0.225 - 45.842i$, $\psi_2 = 0.0053$, $\psi_3 = -1.685$, $\psi_4 = -0.0001$.

According to the Routh-Hurwitz criterion, we note that all the eigenvalues associated with this characteristic polynomial are complex and complex conjugate with positive real parts, except for one single real solution with negative sign. Therefore we can conclude that P_1 is an unstable equilibrium point too.

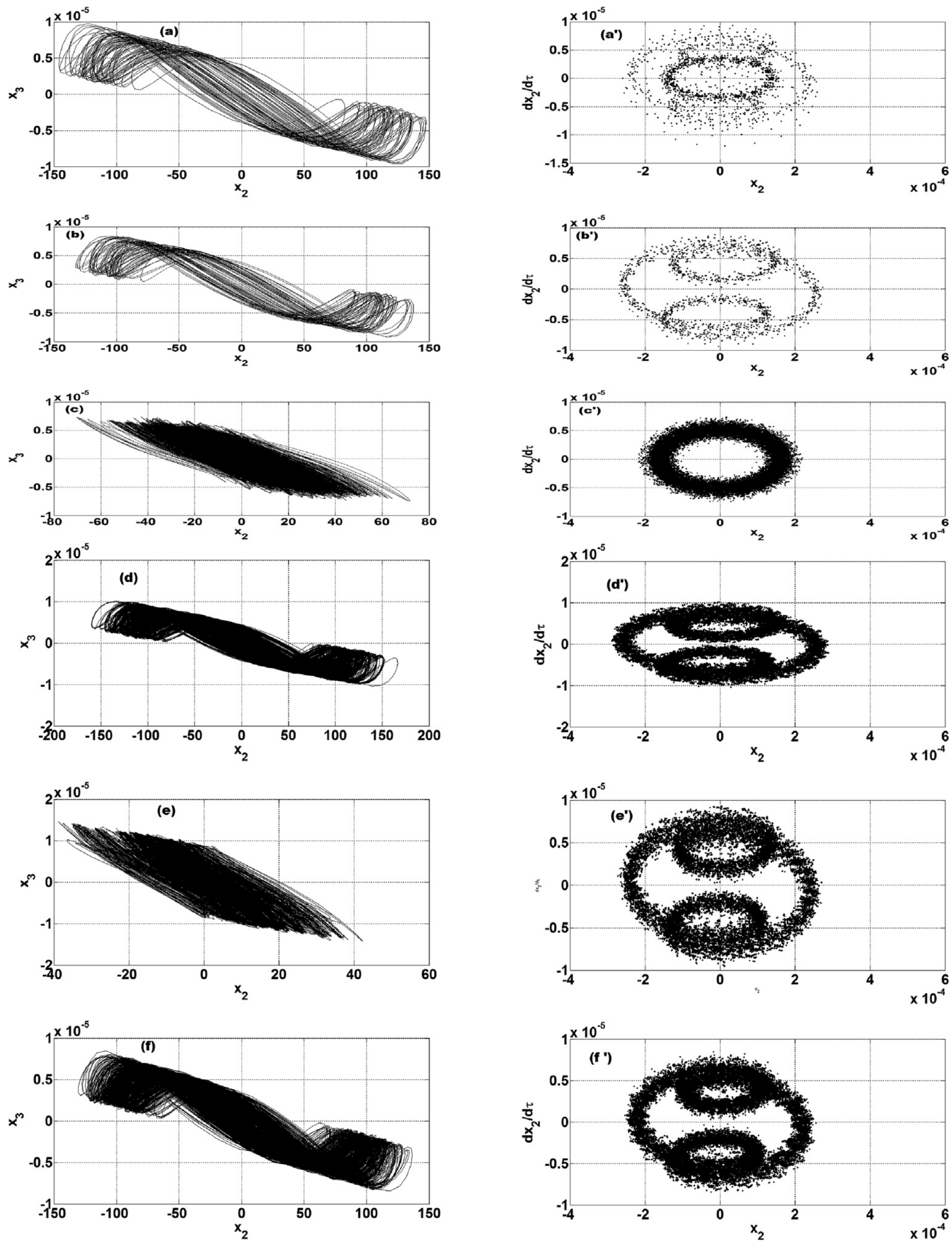

Figure 13. Representation of phase portraits $x_3 = f(x_2)$ left and the corresponding Poincaré map sections $\frac{dx_2}{d\tau} = f(x_2)$ (right) (a-a') and (b-b') are signature of chaos for $\eta = 78.75$(equivalent to $C_1 = 97.68$nF), respectively $\eta = 85(C_1 = 90.49$nF); (c-c') and (d-d') depict hyperchaos type 1 for $\eta = 50$(or $C_1 = 153.84$nF), respectively $\eta = 80$(or $C_1 = 96.1$nF); (e-e') and (f-f') denote hyperchaos type 2 for $\eta = 84.06$(or $C_1 = 91.5$nF), and $\eta = 95$(or $C_1 = 80.9$nF) respectively.

3. Numerical, analog and experimental results

3.1. MATLAB simulations

3.1.1. Non periodic behavior

The dynamics of the new oscillator can be figured out using the plot of the local maximum $x_3(\tau)$ versus the control parameter η. Considering therefore the following set of initial conditions for the system $X_0 = (0.65, 0.75, 0.65, 0.08, 0.08)$ and varying the control parameter η in the range of $30 \leq \eta \leq 100$ while affecting to other parameters the values $\alpha = 10^4$, $\beta = 10^{-4}$, $\theta = 8.93$, $\xi = 24.96$, $\overline{\xi} = 3.92 \times 10^{-6}$, $\overline{\eta} = 0.45$, $\gamma = 2.04$, and $a_0 = 10^{20}$, we obtain the bifurcation diagrams in Figure 7(a). One can have the confusing impression that there are windows of regularities on the bifurcation diagram. A zoom of the bifurcation diagram (Figure 7(b)) for a tiny value of $x_3(\tau)$ and just for $98 \leq \eta \leq 100$ out of $30 \leq \eta \leq 100$ reveals that the apparent windows of regularities on Figure 7(a) are hiding a different dynamics. The graphical result below shows another magnified bifurcation diagram of chaotic type, which reinforces the assertion that the circuit is permanently either chaotic, hyperchaotic or both. To confirm that assertion, let's calculate the maximal Lyapunov exponent:

The numerically computation of the maximum Lyapunov of the system

$$\lambda_{max} = \lim_{x \to +\infty} \frac{1}{n} \sum_{i=0}^{n-1} \ln\left|f'(x_i)\right| \tag{28}$$

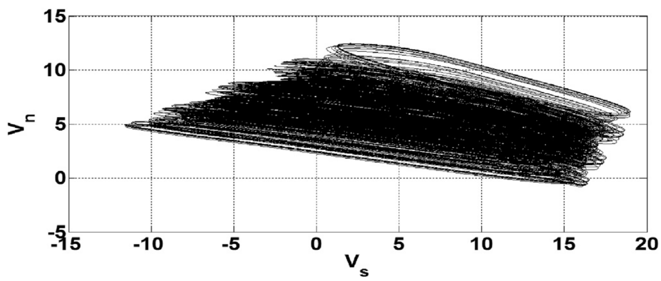

Figure 14. Chaotic attractor obtained with the P-Spice simulator. The voltage at the inverting input (V_n) is represented as a function of the output voltage (V_s) of the operational amplifier for $L_1 = 1mH$; $C_1 = 99.25nF$ ($\eta = 77.50$), $C_2 = 340nF$.

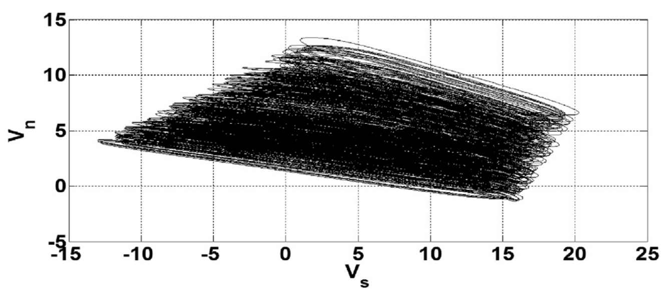

Figure 15. Hyper-chaotic attractor obtained with the P-Spice simulator. The voltage at the inverting input is represented as a function of the output voltage of the operational amplifier for; $L_1 = 1mH$; $C_1 = 91.5nF$ ($\eta = 84.06$), $C_2 = 340nF$.

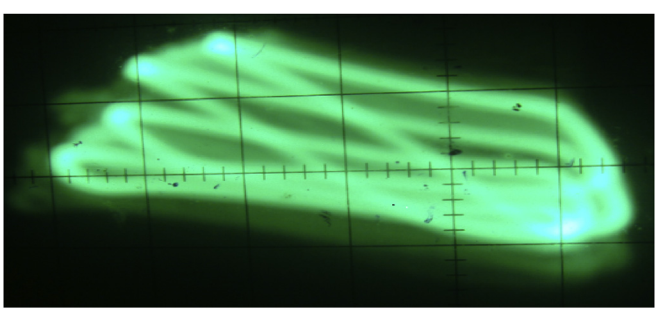

Figure 16. Chaotic attractor of the new Colpitts oscillator; representing the voltage at the non-inverting input (V_n) as a function of the output voltage (V_s) with (X: 0.2 V/Div, Y: 0.5 V/Div). The operational amplifier used is UA741 type, biased with$\pm$15VDC voltage and the values of the circuit components values of $L_1 = 2mH$; $C_1 = 92nF$ ($\eta = 83.6$); $C_2 = 410nF$.

is necessary to explored the nature of its dynamics. Here, *n* is the number of iteration and

$$f'(x_i) = M_j \times u_i \tag{29}$$

with $u_i (i = 1, 2, 3, 4, 5)$ the local variables used to describe the dynamics of system (5). The result obtained under the same initial conditions and set of parameters values as for the previous figure is depicted by Figure 8.

The multitude of points on the bifurcation diagram Figure 7 gives to imagine the absence of periodic behavior in the system. This assumption is confirmed by the sign of the maximum Lyapunov $\lambda_{max} > 0$, showing that the system is always chaotic or hyperchaotic and exhibits neither limit cycles, nor multiperiodic attractors. Figure 9 depicts an example of chaotic attractors plotted for $\eta = 77.50$, which corresponds to $\lambda_{max} = 0.1088$.

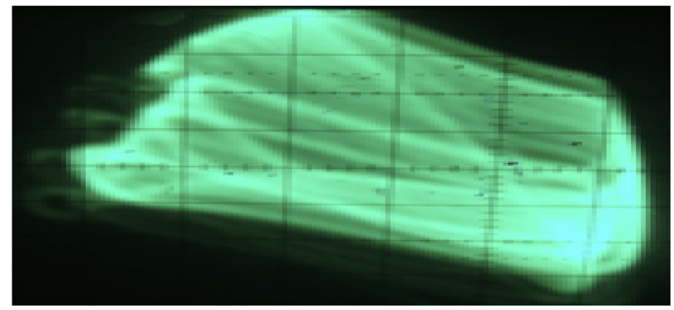

Figure 17. Hyper-chaotic attractor of the new Colpitts oscillator; representing the voltage at the non-inverting input (V_n) as a function of the output voltage (V_s) with (X: 0.2 V/Div, Y: 0.5 V/Div). The operational amplifier used is UA741 type, biased with$\pm$15VDC voltage and the values of the circuit components values of $L_1 = 2mH$; $C_1 = 120nF$ ($\eta = 64.1$); $C_2 = 410nF$. This corresponds to an hyperchaotic attractor of type 1 where $\lambda_2 > 0$and.$\lambda_3 > 0$.

3.1.2. Bistability in the resistorless Op-Amp based oscillator

According to Sprott and Li, the importance of multistability resides in the fact that it is a common phenomenon in nature which, in practical engineering, can lead to unexpected and disastrous consequences [52]. Due to this importance, there is an intensive and active research on the topic [53, 54, 55].

It is nevertheless worth mentioning that mutistability also has advantages in some practical applications. For instance, it has been reported in electronic engineering that changes in initial conditions of versatile analog signal generators can be exploited to alter the type of oscillations [52]. Zeng et al. have shown that mutistability in neural network applications can be applied to enhance the storage capacity of associative memories [56].

Through a forwards and a backwards sweep of the parameter in the range $30 \leq \eta \leq 100$ for two closed initial conditions $x_{01} = (0.65, 0.75, 0.65, 0.08, 0.08)$ for the black color and $x_{02} = (0.065, 0.075, 0.065, 0.008, 0.008)$ for red color, different bifurcation pattern Figure 10 are obtained. The same set of parameters as in the previous sections has been used in both cases. Since the change in initial conditions of the system also implies change in the bifurcation pattern, it means there is a coexistence of different attractors for each value of the control parameter η [14, 57]. Thus, the existence of bistability in our asymmetric system (5) is confirmed [52]. It is remarkable that this phenomenon usually obtained in complex neural networks can also be observed in this simple Op-Amp-based oscillator.

3.1.3. Coexistence of chaos and hyperchaos

Consider again the set of initial conditions $x_{01} = (0.65, 0.75, 0.65, 0.08, 0.08)$ previously chosen in subsection 3.1 to generate the bifurcation diagram in Figure 7. Let us plot the corresponding Lyapunov spectrum Figure 11(a) where λ_i $(i = 1, 2, 3, 4, 5)$ are respectively depicted with green, red, braun, rosa and blue colors. λ_1 (green) is largely negative (Figure 11(b)), so that the sum of all the λ_i is always negative. λ_2 (red) is always positive (Figure 11(c)), accounting that the system doesn't exhibit periodic or multiperiodic oscillations, but is always at least chaotic. λ_3 (braun) and λ_4 (rosa) are negative and positive respectively as the control parameter increases from $\eta = 30$ upwards. At $\eta = 73.98$, λ_4 takes briefly the value zero, then increases again to drop to zero once more at $\eta = 75.86$, remains negative and jumps to positive at $79.93 \leq \eta \leq 80.40$. From there, it remains definitely negative as η increases. The same scenario in reverse is observed by λ_3 It starts with negative value and becomes positive for $83.61 \leq \eta \leq 84.10$, then returns to negative in the window $84.10 \leq \eta \leq 86.35$. The last negative window is situated at $88.62 \leq \eta \leq 89.64$, from where λ_3 will remains always positive (Figure 11(d)). We notice that almost all the time along the path, λ_2 and λ_3 (type 1) or λ_2 and λ_4 (type 2) are always positive, so that the system exhibits hyperchaos of type 1 for the control parameter values $\eta \in [30.00\ ;\ 73.98[\cup]73.98\ ;\ 75.86[\cup]\ 79.93\ ;\ 80.40[$and of type 2 for $\eta \in]83.61\ ;\ 84.10[\cup]86.35\ ;\ 88.62[\cup]89.64\ ;\ 100.00]$. Else is the system chaotic since $\lambda_2 > 0$, always. Finally λ_5 (blue color) is also always negative (Figure 11(e)).

Figure 12 depicts the chaotic and hyperchaotic regions type 1 and 2 according to the values taken by η and to the sign of λ_2, λ_3 and. λ_4.

Figure 12 confirms that the high frequency Colpitts oscillator produces hyper-chaotic oscillations because we can see that the latter has at least two positive Lyapunov exponents at the same time except in the range of purely chaotic oscillations and two negative Lyapunov exponents. There are also zero crossing areas of $\lambda_3$andλ_4. Moreover the sum of all the Lyapunov exponents is always negative independently on the value of η. Similarly for some values of the control parameter η taken in the range of hyper-chaotic oscillations, we represent for some selected points in these zones, the Poincare map sections Figure 13 and the corresponding phase portraits of the dynamic system (4).

For some chosen values of the control parameter in the chaotic regions (Figs. 13(a) and (b)) respectively hyperchaotic regions (Figs 13(c)–(f)), we expose phase diagrams and the corresponding Poincaré sections, all simulated under the same initial conditions and parameters, except for the control parameter which varies in the range $30 \leq \eta \leq 100$.

3.2. Analog results

To proceed with Pspice simulations, we choose the UA741 Op-Amp model and biased it with a DC voltage of $V_{CC} = \pm 15V$. Other components' values of the circuit were$L_1 = 1mH$;$C_1 = 99.25nF$$C_2 = 340nF$. The chaotic attractor of Figure 14 gives the graphical result.

Changing the value of the controlling element to $C_1 = 91.5nF$ and maintaining the previous values for the other components, the system fell into hyperchaotic oscillations characterized by the attractor of Figure 15.

Fig. 14 and Fig. 15 confirm that there is indeed coexistence between the chaotic and hyper-chaotic oscillations in the present microwave oscillator.

3.3. Experimental results

During the laboratory experimental study, we used again the general purpose operational amplifier type UA741 biased at $V_{CC} = \pm\ 15V$. The components for the resonator were worth: $L_1 = 2mH$; $10nF \leq C_1 \leq 410nF$; $C_2 = 410nF$. The chaotic attractor obtained is depicted by Figure 16.

An increase of the value of the external capacitor to $C_1 = 120nF$ led to hyperchaos, Figure 17. We notice that the control parameter η depends on the capacitor C_1, and that chaos and hyperchaos emerge from the parameter ranges predicted by the theory.

4. Conclusion

In the framework of a project called "simple circuits with unexpected high degree of freedom", we have reported a microwave oscillator, made solely of a general purpose Op-Amp and a Colpitts resonator. This simplest Op-Amp-based Colpitts circuit is described by an asymmetric system and depicts complex dynamics that are usually observed in more complex systems such as bistability [52]. In the contrary of the circuit of Ref. [28] which exhibits only chaotic signals, in the present oscillator, we report coexistence of both chaotic and hyper-chaotic oscillations. The particularity lies in its nonlinear amplifier which is totally different from all the others' models encountered in the literature. Mostly, the existing models place an emphasis on negative resistance to inject nonlinearity into the feedback loop. This simple oscillator (looking the number of components) exhibits a dynamic that was previously unsuspected. Furthermore, it could be noted that in the presence of high frequencies and strongly nonlinear signals, a general purpose Op-Amp with voltage feedback (VFA) characteristics can adopt a behavior which is reserved to Op-Amps with current feedback (CFA).

Indeed our circuit presents good characteristics of oscillators solicited to secure information in telecommunication such as chaos, hyper-chaos and bistability. Because of its simplicity, we think that its implementation for engineering applications should not cause any difficulty. Furthermore, it validates the high frequency model of general purpose Op-Amp recently proposed by Tchitnga et ***al***. [42]. The simplicity of the circuit predisposes it to be used as didactic material to introduce coexistence of chaos and hyperschaos, bistability and other features of complex systems, at undergraduate Level.

Looking at the relevance of the results presented in this paper, we launch an appeal to reconsider some existing works on high frequency chaotic oscillators based on the operational amplifiers [58, 59] at the light of the high frequency model of general purpose Op-Amp in Ref. [42], as we believe these authors would have missed many interesting phenomena by considering the Op-Amp as operating at low frequency. A next outcome of the present paper is the study of the fractional model of our model oscillator.

Declarations

Author contribution statement

R. Zebaze Nanfa'a: Performed the experiments; Analyzed and interpreted the data; Wrote the paper.

R. Tchitnga: Conceived and designed the experiments; Analyzed and interpreted the data; Contributed reagents, materials, analysis tools or data; Wrote the paper.

P. H. Louodop Fotso, R. Kengne: Analyzed and interpreted the data.

C. F. Talla: Performed the experiments.

B. Nana: Performed the experiments; Wrote the paper.

F.B. Pelap: Contributed reagents, materials, analysis tools or data.

Funding statement

This research did not receive any specific grant from funding agencies in the public, commercial, or not-for-profit sectors.

Competing interest statement

The authors declare no conflict of interest.

Additional information

No additional information is available for this paper.

References

[1] M. Brucoli, D. Cafagna, L. Carnimeo, G. Grassi, Synchronization of hyperchaotic circuits via continuous feedback control with application to secure communications, Int. J. Bifurcat. Chaos 8 (10) (1998) 2031–2040.
[2] G. Grassi, S. Mascolo, A system theory approach for designing cryptosystems based on hyperchaos, IEEE Transanct. Circ. Syst. 46 (9) (1999) 1135–1138.
[3] C. Li, Y. Liu, T. Xie, M.Z. Chen, Breaking a novel image encryption scheme based on improved hyperchaotic sequences, Nonlinear Dynam. 73 (3) (2013) 2083–2089.
[4] Z. Hua, S. Yi, Y. Zhou, C. Li, Y. Wu, Designing hyperchaotic cat maps with any desired number of positive Lyapunov exponents, IEEE Transanct. Cybern. 48 (2) (2018) 463–473.
[5] K. Thamilmaran, M. Lakshmanan, A. Venkatesan, Hyperchaos in a modified canonical Chua's circuit, Int. J. Bifurcat. Chaos 14 (1) (2004) 221–243.
[6] S. Nikolov, S. Clodong, Hyperchaos–chaos–hyperchaos transition in modified Rössler systems, Chaos, Solit. Fractals 28 (1) (2006) 252–263.
[7] Y. Chen, Q. Yang, A new Lorenz-type hyperchaotic system with a curve of equilibria, Mathematics and, Computers in Simulation 112 (2015) 40–55.
[8] K. Murali, A. Tamasevicius, G. Mykolaitis, A. Namajunas, E. Lindberg, Hyperchaotic system with unstable oscillators, Nonlinear Phenom. Complex Syst. Minsk 3 (1) (2000) 7–10. http://orbit.dtu.dk/files/2419460/oersteddtu1788.pdf. Accessed on 03/05/2019, 13:47.
[9] A. Čenys, A. Tamaševičius, A. Baziliauskas, R. Krivickas, E. Lindberg, Hyperchaos in coupled Colpitts oscillators, Chaos, Solit. Fractals 17 (2-3) (2003) 349–353.

[10] B. Cannas, S. Cincotti, Hyperchaotic behaviour of two bi-directionally coupled Chua's circuits, Int. J. Circ. Theor. Appl. 30 (6) (2002) 625–637.
[11] M. Ahmad, Al.E. Solami, X.Y. Wang, M. Doja, M. Beg, A. Alzaidi, Cryptanalysis of an image encryption algorithm based on combined chaos for a BAN system, and improved scheme using SHA-512 and hyperchaos, Symmetry 10 (7) (2018) 266.
[12] A. Balamurugan, V. Sengodan, Period doubling routes to hyper chaos in a new non-source free nonlinear circuit with diodes, Int. J. Electron. Eng. 3 (2) (2011) 173–175. http://csjournals.com/IJEE/PFD3-2/4-_A._Balamurugan.pdf. Accessed on 03/05/2019, 13:56.
[13] U.E. Vincent, B.N. Nbendjo, A.A. Ajayi, A.N. Njah, P.V. McClintock, Hyperchaos and bifurcations in a driven Van derPol–Duffing oscillator circuit, Int. J. Dynam. Contr. 3 (4) (2015) 363–370.
[14] Z. Wei, I. Moroz, J.C. Sprott, A. Akgul, W. Zhang, Hidden hyperchaos and electronic circuit application in a 5D self-exciting homopolar disc dynamo, Chaos 27 (3) (2017) 1–10.
[15] R. Tchitnga, B.A. Mezatio, T. Fozin, R. Kengne, P.H.F. Louodop, A. Fomethe, A novel hyperchaotic three-component oscillator operating at high frequency, Chaos, Solit. Fractals 118 (2019) 166–180.
[16] L.O. Chua, The Genesis of Chua's Circuit 46, Hirzel-Verlag, Stuttgart, 1992, pp. 250–257 (4), https://www.inst.cs.berkeley.edu/~ee129/sp10/handouts/GenesisChuasCircuit.pdf. Accessed on 03/05/2019, 14:03.
[17] R. Tchitnga, H.B. Fotsin, B. Nana, P.H.L. Fotso, P. Woafo, Hartley's oscillator: the simplest chaotic two-component circuit, Chaos, Solit. Fractals 45 (3) (2012) 306–313.
[18] C. Aissi, Introducing chaotic circuits in an undergraduate electronic course, in: Proceedings of the 2002 ASEE Gulf-Southwest Annual Conference, the University of Louisiana at Lafayette, 2002 March 20, pp. 1–8.
[19] M.A. Perc, Introducing nonlinear time series analysis in undergraduate courses, FIZIKA A-ZAGREB 15 (2) (2006) 91–112. http://fizika.hfd.hr/fizika_a/av06/a15p091.pdf. Accessed on 18/06/2019; 11:41.
[20] F.C. Talla, R. Tchitnga, R. Kengne, B. Nana, A. Fomethe, Didactic model of a simple driven microwave resonant T-L circuit for chaos, multistability and antimonotonicity, Heliyon 5 (2019), 02715.
[21] R. Kengne, R. Tchitnga, A. Mezatio, A. Fomethe, G. Litak, Finite-time synchronization of fractional-order simplest two-component chaotic oscillators, Eu. Phys. J. B 90 (5) (2017) 88.
[22] S.T. Kingni, G.F. Kuiate, V.K. Tamba, V. Pham, D.V. Hoang, Self-excited and hidden attractors in an autonomous josephson jerk oscillator: analysis and its application to text encryption, ASME, J. Comput. Nonlinear Dynam. 14 (7) (2019), 071004.
[23] R.M. Nguimdo, R. Tchitnga, P. Woafo, Dynamics of coupled simplest chaotic two-component electronic circuits and its potential application to random bit generation, Chaos: An Interdiscipl. J. Nonlinear Sci. 23 (4) (2013), 043122.
[24] M.E. Yalcin, J.A. Suykens, J. Vandewalle, True random bit generation from a double-scroll attractor, IEEE Transact. Circ. Syst. I: Regul. Pap. 51 (7) (2004) 1395–1404.
[25] J.G. Freire, J.A. Gallas, Cyclic organization of stable periodic and chaotic pulsations in Hartley's oscillator, Chaos, Solit. Fractals 59 (2014) 129–134.
[26] M. Kountchou, V.F. Signing, R.T. Mogue, J. Kengne, P. Louodop, Saïdou, Complex dynamic behaviors in a new Colpitts oscillator topology based on a voltage comparator, AEU-Int. J. Electron. Commun. (2020) 153072.
[27] P. Louodop, S. Saha, R. Tchitnga, P. Muruganandam, S.K. Dana, H.A. Cerdeira, Coherent motion of chaotic attractors, Phys. Rev. 96 (4) (2017) 42210.
[28] W. San-Um, B. Suksiri, P. Ketthong, A simple RLCC-diode-opamp chaotic oscillator, Int. J. Bifurcat. Chaos 24 (12) (2014) 1–8.
[29] J.C. Sprott, A proposed standard for the publication of new chaotic systems, Int. J. Bifurcat. Chaos 21 (9) (2011) 2391–2394.
[30] Colpitts E.H., Wireless telegraphy and telephony, U.S. Patent 1 (1918) 256-983. https://patents.google.com/patent/US1624537A/en (Accessed on 03/05/2019, 14:11).
[31] E. Lindberg, K. Murali, A. Tamasevicius, The Colpitts oscillator family, NPW 2008 (2008) 47–48. https://pdfs.semanticscholar.org/bf23/0626d03410242751148f500354b785ea085f.pdf. Accessed on 03/05/2019, 14:13.
[32] N. Swarupa, Design and simulation of chaotic colpitt's oscillator, in: ICECA, IEEE, 2018, pp. 1505–1508. ID:8474857.
[33] V.T. Kamdoum, H.B. Fotsin, J. Kengne, et al., Complex dynamical behavior of a two-stage Colpitts oscillator with magnetically coupled inductors, J. Chaos 2014 (2014) 1–11. ID:945658.
[34] C. Su, S. Thoka, K.C. Tiew, R.L. Geiger, A 40 GHz modified-Colpitts voltage controlled oscillator with increased tuning range, in: Proceedings of the 2003 International Symposium on Circuits and Systems (ISCAS'03), 1, IEEE, 2003, 1-1.
[35] M.M. Jakas, F. Llopis, LC sine-wave oscillators using general-purpose voltage operational-amplifiers, Int. J. Electr. Eng. Educ. 44 (3) (2007) 244–248.
[36] A. Leven, Telecommunication Circuits and Technology, Book, Elsevier, 2000.
[37] R.L. Boylestad, L. Nashelsky, Electronic Devices and Circuit Theory, Prentice Hall, Upper Saddle River, New Jersey Columbus, Ohio, 2012. https://lib.hpu.edu.vn/handle/123456789/21368. Accessed on 03/05/2019, 15:06.
[38] A.S. Elwakil, M.P. Kennedy, A family of colpitts-like of chaotic oscillators, J. Franklin Inst. 336 (4) (1999) 687–700.
[39] T. Banerjee, B. Karmakar, B.C. Sarkar, Chaotic electronic oscillator from single amplifier biquad, Int. J. Electron. Commun. 66 (7) (2012) 593–597.
[40] R. Samanbakhsh, A. Taheri, Reduction of power electronic components in multilevel converters using new switched capacitor-diode structure, IEEE Trans. Ind. Electron. 63 (11) (2016) 7204–7214.
[41] T. Ramakrishnan, R. Sornalatha, High speed and efficient power reduction in pulse triggered flipflop based on signal feed through scheme, Int. J. Res. Appl. Sci. Eng. Technol. 3 (1) (2015) 1–5. https://www.ijraset.com/fileserve.php?FID=2522.
[42] R. Tchitnga, R.N. Zebaze, F.B. Pelap, P. Louodop, P. Woafo, A novel high-frequency interpretation of a general purpose Op-Amp-based negative resistance for chaotic vibrations in a simple a priori non chaotic circuit, J. Vib. Contr. 23 (5) (2017) 744–751.
[43] G.-S. Yim, J.-W. Ryu, Y.-J. Park, S. Rim, S.-Y. Lee, W.-H. Kye, C.-M. Kim, Chaotic behaviors of operational amplifiers, Phys. Rev. E. 69 (4) (2004), 045201.
[44] G. Breed, Fundamentals of passive component behavior at high frequencies, High Freq. Electron. (2006) 16–22. http://www.highfrequencyelectronics.com/Jun06/HFE0606_Tutorial.pdf. Accessed on 03/05/2019, 15:39.
[45] R.C. Toonen, S.P. Benz, Nonlinear behavior of electronic components characterized with precision multitones from a Josephson arbitrary waveform synthesizer, IEEE Trans. 19 (3) (2009) 715–718.
[46] J. Karki, Effect of Parasitic Capacitance in Op Amp Circuits- Mixed Signal Products(Application Report, White Paper: SLOA013A), Texas Instruments, Dallas, Texas, 2000. Available at: http://www.ti.com.cn/cn/lit/an/sloa013a/sloa013a.pdf. Accessed 03/05/2019, 15:40.
[47] C. Wolff, J.G. Kenney, L.R. Carley, CAD for the analysis and design of ΔΣ converters, in: Delta-sigma Data Converters: Theory, Design and Simulation, IEEE Press, 1997, pp. 447–467.
[48] A. Rana, P. Gaikwad, Colpitts oscillator: design and performance optimization, Int. J. Appl. Sci. Eng. Res. 3 (5) (2014) 913–919.
[49] W. Jung, Op Amp Applications Handbook, Elsevier, Burlington, 2005.
[50] L.A. Aguirre, Á.V. Souza, An algorithm for estimating fixed points of dynamical systems from time series, Int. J. Bifurcat. Chaos 8 (11) (1998) 2203–2213.
[51] C.G. Boehmer, T. Harko, S.V. Sabau, Jacobi stability analysis of dynamical systems-applications in gravitation and cosmology, Adv. Theor. Math. Phys. 16 (4) (2012) 1145–1196. https://projecteuclid.org/download/pdf_1/euclid.atmp/1408559162. Accessed 03/05/2019, 15:51.
[52] J.C. Sprott, C. Li, Asymmetric bistability in the rössler-system, acta, Phys. Pol. B 48 (1) (2017). http://sprott.physics.wisc.edu/pubs/paper447.pdf. Accessed 03/05/2019, 15:58.
[53] E.M. Ngouonkadi, H.B. Fotsin, P.L. Fotso, V.K. Tamba, H.A. Cerdeira, Bifurcations and multistability in the extended Hindmarsh–Rose neuronal oscillator, Chaos, Solit. Fractals 85 (2016) 151–163.
[54] A. Taher Azar, N.M. Adele, T. Alain, R. Kengne, F.H. Bertrand, Multistability analysis and function projective synchronization in relay coupled oscillators, Hindawi Complex. 2018 (2018) 1–12.
[55] P. Louodop, R. Tchitnga, F.F. Fagundes, M. Kountchou, V.K. Tamba, H.A. Cerdeira, Extreme multistability in a Josephson-junction-based circuit, Phys. Rev. 99 (4) (2019), 042208.
[56] Z. Zeng, T. Huang, W.X. Zheng, Multistability of recurrent neural networks with time-varying delays and the piecewise linear activation function, IEEE Transact. 21 (8) (2010) 1371–1377.
[57] Z.T. Njitacke, J. Kengne, Antimonotonicity, chaos and multiple coexisting attractors in a simple hybrid diode-based jerk circuit, Chaos, Solit. Fractals 105 (2017) 77–91.
[58] A.S. Elwakil, M.P. Kennedy, High frequency Wien-type chaotic oscillator, Electron. Lett. 34 (12) (1998) 1161–1162.
[59] A. Kordonis, Y. Nakakohara, H. Otake, Chaotic triangle Wave Generator Implementing Chua Circuit towards DC/DC Converter Control, Enoc, Budapest, Hungary, 2017. https://congressline.hu/enoc2017/abstracts/31.pdf. Accessed03/05/2019, 16:06.